J. Fluid Mech. (2003), *vol.* 494, *pp.* 255–274.
DOI: 10.1017/S0022112003006086 Printed in the United Kingdom

On inwardly propagating high-Reynolds-number axisymmetric gravity currents

By MARK HALLWORTH[1], HERBERT E. HUPPERT[1] AND MARIUS UNGARISH[2]

[1]Institute of Theoretical Geophysics, Department of Applied Mathematics and Theoretical Physics, University of Cambridge, Wilberforce Rd, Cambridge CB3 0WA, UK

[2]Department of Computer Science, Technion, Haifa 32000, Israel

(Received 26 August 2002 and in revised form 8 July 2003)

The behaviour of an axisymmetric inviscid gravity current, which is released from a lock near the outer wall of a circular container and then propagates towards the centre over a horizontal boundary, is considered. Shallow-water and box-model theoretical analyses and experimental results are presented and compared. The resulting motion predicted by the shallow-water model displays interesting differences with the previously reported outward propagation of an axisymmetric current, as well as with propagation in a two-dimensional rectangular geometry. The current initially develops the usual decelerating motion with a nose-up tail-down shape, but when the nose reaches about half of the outer radius the confining geometry opposes the further decrease of the height and velocity of the nose. The box-model approximation, which omits the inclination of the interface, is unable to reproduce the hindering (and eventual reversal) effect of the geometrical confinement on the decrease of the nose velocity during the inward propagation.

1. Introduction

Gravity currents occur whenever fluid of one density flows primarily horizontally into fluid of a different density. Many such situations arise in both industrial and natural settings, as reviewed by Simpson (1997) and Huppert (2000). Commonly, the current is driven by compositional or temperature differences, or by suspended particulate matter (Bonnecaze, Huppert & Lister 1993; Bonnecaze *et al.* 1995; Huppert 1998), and combinations of both particle and compositional or temperature differences can also occur (Hogg, Hallworth & Huppert 1999). Currents may propagate in either a rectangular two-dimensional or cylindrical axisymmetric configuration, or may be otherwise influenced by sidewall and/or topographic constraints. Some of these processes have now been fairly well investigated. A typical investigation considers the instantaneous release of a constant volume of heavy fluid from behind a lock into a large reservoir of a less-dense homogeneous fluid above an impermeable horizontal boundary.

A distinction must be made between viscous and inviscid currents, i.e. low- and high-Reynolds-number flows. The propagation in the former case is governed by a viscous–pressure balance and practically independent of the conditions at the nose (Huppert 1982). Viscous gravity currents have been studied in two-dimensional rectangular and axisymmetric divergent (outward propagation) configurations (Huppert 1982 and others), and also in axisymmetric convergent (inward propagation) configurations

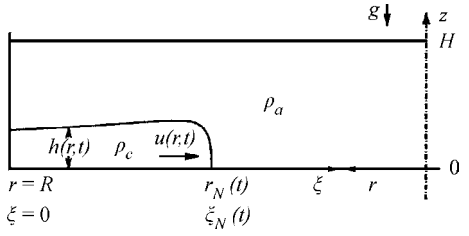

FIGURE 1. Schematic description of the system.

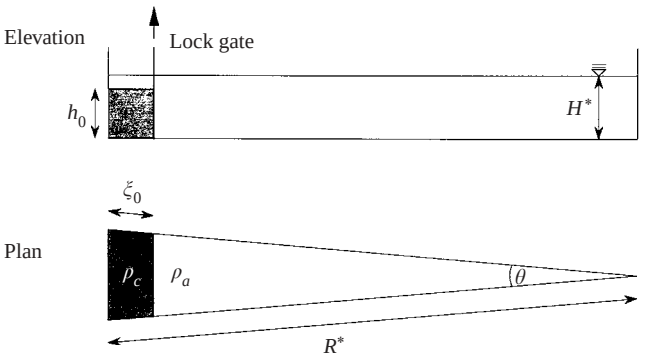

FIGURE 2. Sketch of the experimental sector tank.

(Diez, Gratton & Gratton 1992; Abgenent & Aronson 1995; and others). Pertinent similarity solutions of either the first or second kind (Barenblatt 1966) as appropriate were presented for all cases. On the other hand, the propagation of an inviscid gravity current is governed by an inertia–pressure balance and strongly affected by the conditions at the nose (Benjamin 1968). The classical problems of release of high-Reynolds-number currents from behind a lock concern either non-divergent (two-dimensional rectangular) or positively divergent (axisymmetric radial outward) flows. In these cases self-similar solutions become relevant after a sufficiently long time of propagation. In the axisymmetric convergent configurations another length scale is introduced and therefore similarity solutions of the first kind cannot exist. Similarity solutions of the second kind can be expected to exist in this case, but they will yield information only close to the apex; this topic is under investigation and will be considered in a separate paper.

Our aim here is primarily to evaluate the behaviour of high-Reynolds-number currents in a converging axisymmetric radial inward flow. We show some interesting, perhaps unexpected, differences with the classical cases.

The configuration of the resulting current is shown in figures 1 and 2. An axisymmetric container or sector of radius R^* contains an inner lock of height h_0 at radius $R^* - \xi_0$. (The asterisk is used to denote that here R and H are dimensional, in contrast to later use following the scaling (2)). The space between the lock and the outer radius is initially filled with fluid of density ρ_c. The space outside the lock is filled with ambient fluid of density ρ_a ($< \rho_c$). The free surface of the fluid is at height H^*. We consider cases in which $h_0 < H^*$, which indicates that the ambient fluid is at least at the level of the dense fluid or covers it. At time $t = 0$ the lock is quickly lifted and the dense fluid propagates as a gravity current into the ambient,

in an inward radial direction, i.e. from the periphery towards the centre. We assume that the viscous effects of the global motion can be neglected. Our objective is to analyse the motion, in particular the velocity of propagation and the shape of the interface. The novelty is in the direction of propagation. The change of direction of the motion has some interesting consequences.

The major motivation was academic curiosity concerning the behaviour of gravity currents in general circumstances and the predictive powers of models. However, the insights may also be useful in practical circumstances, for example, the understanding of turbidity currents either generated at the peripheral shoreline of a lake and flowing inwardly to its centre or propagating into a convergent canyon.

We use a cylindrical coordinate system, r, θ, z, with the gravitational acceleration g acting in the $-z$-direction. The radial velocity component is denoted by u, and the subscript N denotes the nose of the current. We assume that there is no azimuthal motion (a straightforward consequence of the geometry and initial conditions). The driving factor is the reduced gravity, defined as

$$g' = \frac{\rho_c - \rho_a}{\rho_a} g. \tag{1}$$

The geometrical parameters of the problem are

$$R = R^*/\xi_0, \quad H = H^*/h_0, \tag{2}$$

and it is convenient to scale the dimensional variables (denoted here by asterisks) by

$$\{r^*, \xi^*, z^*, h^*, t^*, u^*\} = \{\xi_0 r, \xi_0 \xi, h_0 z, h_0 h, Tt, Uu\}, \tag{3}$$

where

$$U = (g' h_0)^{1/2}, \quad T = \xi_0/U. \tag{4}$$

Here h_0 and ξ_0 are the dimensional initial height and radial length of the current, U is a typical (dimensional) inertial velocity of propagation of the nose of the current, and T is a typical (dimensional) time period for horizontal propagation over the (dimensional) distance ξ_0.

For subsequent use we introduce the dimensionless inward radial coordinate ξ, measured from the outer boundary towards the axis,

$$\xi = R - r \qquad (0 \leqslant \xi \leqslant R). \tag{5}$$

We consider cases with high Reynolds numbers, in particular $u_N^* h_N^*/\nu \gg 1$, where ν is the kinematic viscosity coefficient, and hence viscous effects can be neglected. Therefore, as proved later, the scaled problem is specified by two dimensionless numbers, the geometrical parameters R and H, which express the ratio of the outer radius to the initial radial length of the current or lock, and the ratio of the total height of the ambient to the initial height of the current or lock.

Our aim was to understand how an inwardly propagating axisymmetric current is influenced by the geometry as it approaches the apex. The answer is not straightforward because it could be argued that as the current spreads the height of the nose must decrease. Alternatively, it might be argued that the constraining geometry leads to an increase in height of the nose. To elucidate this problem in a reliable manner we performed the combined experimental and theoretical work reported here. In our theoretical discussion we show that both arguments are correct: the nose is predicted first to decrease in height, and then increase as the apex is approached.

The structure of the paper is as follows. In the next section the experimental setup and results are presented and discussed. In § 3 we develop the model equations of motion, based on a one-layer shallow-water approximation and the appropriate boundary conditions. In § 4 our theoretical results are compared with the experiment, and also used to develop an understanding for a wider range of R than possible experimentally. We present a summary of our results and some concluding remarks in § 5. The pertinent box-model simplification is also developed in the Appendix.

2. Experiments

The lock-release experiments were carried out in a Perspex sector tank of angle $\theta = 10^\circ$, radius $R^* = 234.1$ cm and depth 40.8 cm, as sketched in figure 2.

The tank could be partitioned by means of a thin removable barrier positioned vertically at some distance ξ_0 from the outer wall. Since both the endwall of the tank and the barrier were straight-sided, the tank was not strictly sector-shaped. However, there is little difference between the perimeter section subtended by an angle of 10° and an equivalent straight chord.

For most experiments, the tank was filled to the desired depth H^* with tap water, and the vertical lock gate was positioned at a distance ξ_0 from the endwall. Known amounts of salt were then dissolved in the water behind the lock to produce the desired density excess. In these cases, the height of the dense layer (h_0) was initially equal to that of the ambient layer, and hence the dimensionless ratio $H = 1$. In other cases, where $H > 1$, the fluid behind the lock was stratified into two layers separated by a sharp, horizontal interface, by carefully floating a layer of fresh water on top of the salt solution using a sponge filling boat. Once any residual filling motion in the fluid had ceased, the lock gate was quickly withdrawn vertically and the dense current spread over the smooth base of the tank towards the apex. A total of 39 experiments were performed with systematic variation of the initial conditions g', ξ_0, h_0 and H, as presented in table 1. In each run, the propagation of the current was recorded by marking the position of the nose (ξ_N) at 3 s time intervals.

We found that all the data could conveniently be collapsed using the length and time scales defined in (3)–(4) for the initial period of propagation, but for later times some scatter appeared. These deviations from the initial pattern can be attributed to viscous effects, which are beyond our scope. Using the measurements, we estimated for each experiment the nose velocity, height and local Reynolds number, as functions of time. (We note that the accuracy of these results is low because of accumulation of measurement errors, yet sufficient for the order-of-magnitude considerations discussed here.) We found that for some experiments the Reynolds number decays to values below 100, which indicates that the viscous bottom friction became important, even dominant, during propagation. These experiments were marked by V in table 1, and hereafter excluded from our discussion. The dimensionless remaining data display a consistent behaviour for the whole range of propagation. An order-of-magnitude analysis indicated that the sidewall friction is much smaller than the total inertial force.

A typical series of results is presented in figure 3(a), which shows the distance of the nose from the outer wall as a function of time from release, for a wide range of variable parameters. Figure 3(b) shows the same data in dimensionless form, using log–log coordinates. This plot displays a fairly good collapse onto a straight line fit of unit slope, which suggests that the velocity of each current was almost constant and of the order of magnitude of the scaling velocity U given by (4).

Expt	H^* (cm)	h_0 (cm)	ξ_0 (cm)	g' (cm s^{-2})	H	ξ_0/h_0	R	U (cm s^{-1})	Re_0 ($\times$ 1000)	ξ_V/R	
1	13.2	13.2	13.2	10.04	1.00	1.00	17.7	11.5	15.2	0.88	
2	13.2	13.2	13.2	5.05	1.00	1.00	17.7	8.2	10.8	0.80	
3	13.2	13.2	13.2	19.74	1.00	1.00	17.7	16.1	21.3	0.97	
4	6.3	6.3	6.3	5.87	1.00	1.00	36.9	6.1	3.9	0.29	V
5	6.3	6.3	6.3	10.71	1.00	1.00	36.9	8.3	5.2	0.31	V
6	6.3	6.3	6.3	20.35	1.00	1.00	36.9	11.4	7.2	0.34	V
7	13.2	13.2	6.3	5.87	1.00	0.48	36.9	8.8	11.6	0.49	V
8	13.2	13.2	6.3	10.69	1.00	0.48	36.9	11.9	15.7	0.53	
9	13.2	13.2	6.3	20.33	1.00	0.48	36.9	16.4	21.6	0.58	
10	6.3	6.3	13.2	5.87	1.00	2.10	17.7	6.1	3.8	4.48	V
11	6.3	6.3	13.2	10.7	1.00	2.10	17.7	8.2	5.2	0.53	
12	6.3	6.3	13.2	20.35	1.00	2.10	17.7	11.3	7.1	0.58	
13	3.2	3.2	6.3	10.65	1.00	2.00	37.2	5.8	1.8	0.19	V
14	9.4	9.4	6.3	10.68	1.00	0.67	37.2	10.1	9.5	0.41	V
15	15.7	15.7	6.3	10.69	1.00	0.40	37.2	13.0	20.4	0.60	
16	6.3	6.3	24.3	5.89	1.00	3.86	9.6	6.1	3.8	0.74	
17	6.3	6.3	24.3	10.71	1.00	3.86	9.6	8.2	5.2	0.81	
18	6.3	6.3	24.3	20.37	1.00	3.86	9.6	11.3	7.1	0.89	
19	13.2	13.2	24.3	5.88	1.00	1.84	9.6	8.8	11.6	1.26	
20	13.2	13.2	24.3	10.71	1.00	1.84	9.6	11.9	15.7	1.38	
21	13.2	13.2	24.3	20.37	1.00	1.84	9.6	16.4	21.6	1.51	
22	3.2	3.2	13.2	10.72	1.00	4.19	17.7	5.8	1.8	0.32	V
23	9.4	9.4	13.2	10.72	1.00	1.40	17.7	10.1	9.5	0.70	
24	15.7	15.7	13.2	10.72	1.00	0.84	17.7	13.0	20.5	1.01	
25	26.4	26.4	13.2	10.72	1.00	0.50	17.7	16.8	44.4	1.46	
26	26.4	15.7	13.2	10.72	1.68	0.84	17.7	13.0	20.5	1.01	
27	26.4	13.2	13.2	10.72	2.00	1.00	17.7	11.9	15.7	0.89	
28	26.4	9.4	13.2	10.72	2.79	1.40	17.7	10.1	9.5	0.70	
29	26.4	6.3	13.2	10.72	4.19	2.10	17.7	8.2	5.2	0.53	
30	26.4	9.4	13.2	10.72	2.79	1.40	17.7	10.1	9.5	0.70	
31	15.7	9.4	13.2	10.72	1.67	1.40	17.7	10.1	9.5	0.70	
32	13.2	9.4	13.2	10.72	1.40	1.40	17.7	10.1	9.5	0.70	
33	21.0	9.4	13.2	10.72	2.22	1.40	17.7	10.1	9.5	0.70	
34	3.2	3.2	10.0	10.72	1.00	3.17	23.4	5.8	1.8	0.26	V
35	6.3	6.3	10.0	10.72	1.00	1.59	23.4	8.2	5.2	0.43	V
36	9.4	9.4	10.0	10.72	1.00	1.06	23.4	10.1	9.5	0.57	
37	13.2	13.2	10.0	10.72	1.00	0.76	23.4	11.9	15.7	0.73	
38	15.7	15.7	10.0	10.72	1.00	0.63	23.4	13.0	20.5	0.83	
39	26.4	26.4	10.0	10.72	1.00	0.38	23.4	16.8	44.4	1.20	

TABLE 1. Experiment data. $Re_0 = Uh_0/\nu$, ξ_V is the theoretical estimate of the end of the inviscid domain (see A 10), and V marks experiments in which the viscous terms are expected to be relatively important during most of the propagation.

Figure 4 shows the measured time of propagation of the nose from the lock to the apex, denoted t_R, as a function of the corresponding distance of propagation, $R - 1$, for various experiments. The fairly linear form of this graph is consistent with the result that the average velocity of the nose was fairly constant for all cases.

An interpretation of the results is deferred until a description of the theoretical investigation is presented in the next section, which includes our experimental range of R and beyond. Our experimental results were restricted to values of R less than 37; larger values would be difficult to obtain experimentally with our tank.

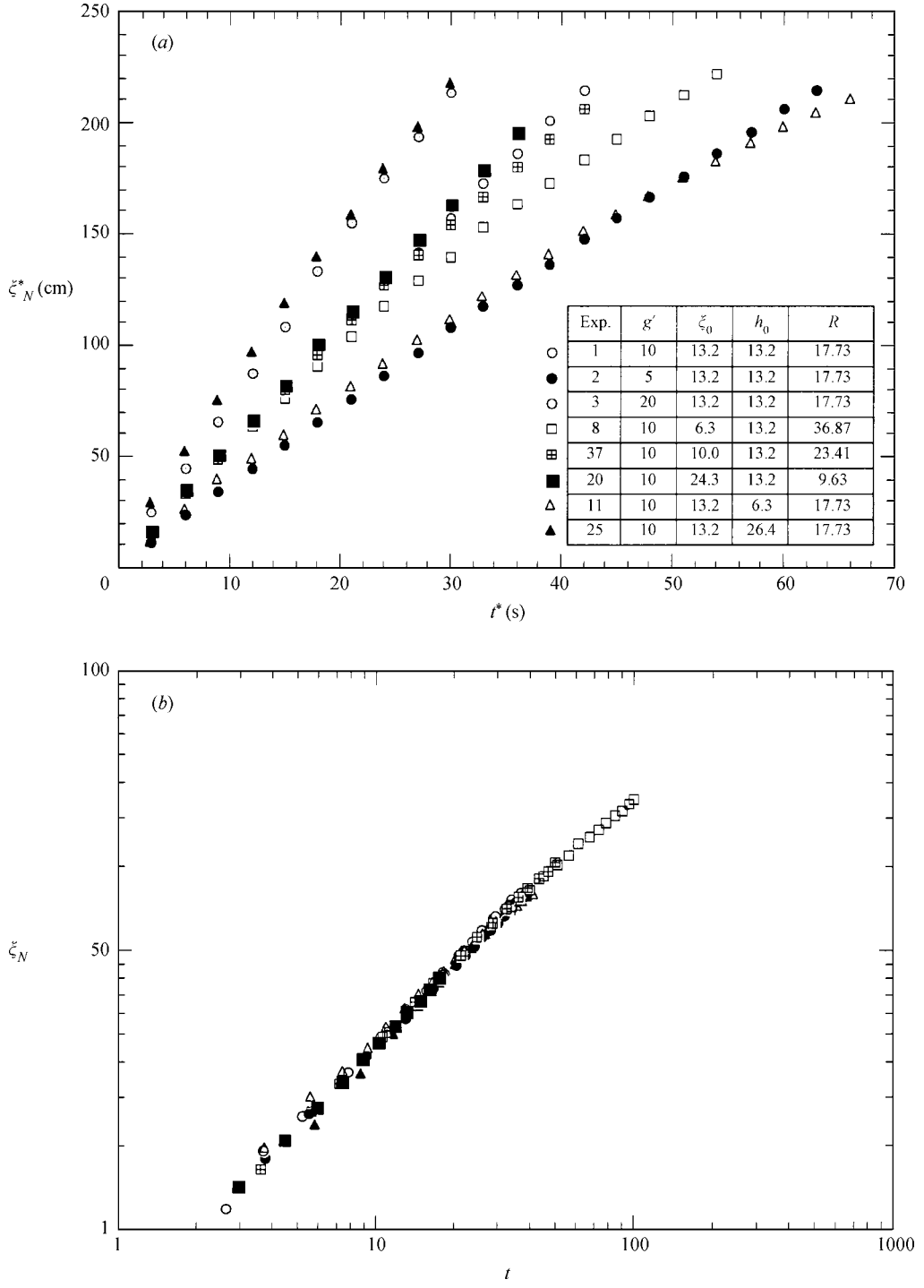

Exp.	g'	ξ_0	h_0	R
1	10	13.2	13.2	17.73
2	5	13.2	13.2	17.73
3	20	13.2	13.2	17.73
8	10	6.3	13.2	36.87
37	10	10.0	13.2	23.41
20	10	24.3	13.2	9.63
11	10	13.2	6.3	17.73
25	10	13.2	26.4	17.73

FIGURE 3. Experimental results for the inward radial displacement of the current as a function of time: (*a*) dimensional coordinates, and (*b*) dimensionless log–log coordinates. In the insert table in (*a*), ξ_0, h_0 and g' are given in c.g.s. units.

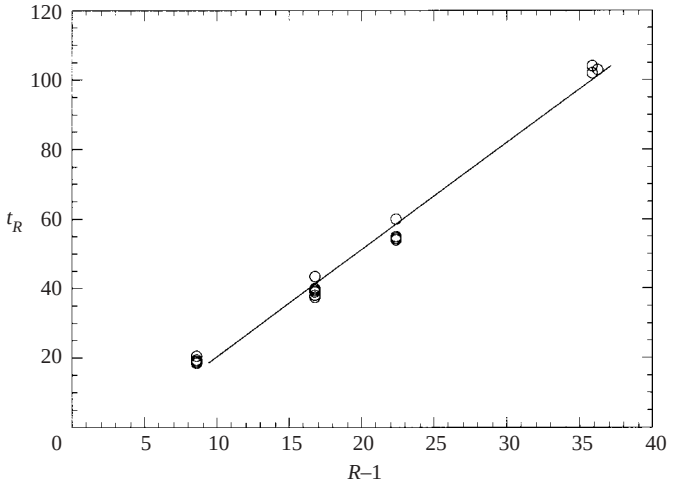

FIGURE 4. Experimental results for the lock-to-apex time of propagation as a function of the corresponding distance $R-1$ in various experiments with $H=1$.

3. Shallow-water (SW) analysis

In terms of the cylindrical coordinate system, r, θ, z, with the gravity acceleration g acting in the $-z$-direction, we develop a one-layer shallow-water (SW) model approximation which is the simplest shallow-water model and is expected to capture many of the important features of the flow. A two-layer model might capture some further details, in particular for shallow-ambient configurations $H<2$ (Klemp, Rotunno & Skamarock 1994; Bonnecaze *et al.* 1995; Ungarish & Zemach 2003), but the analysis and simulations would be more cumbersome; this refinement of our calculations is left for future development. In the ambient fluid domain we assume that the velocity is zero, and hence the fluid is in purely hydrostatic balance. The motion is assumed to take place in the lower layer only, $r_N(t) \leqslant r \leqslant R$ and $0 \leqslant z \leqslant h(x,t)$, which is assumed shallow in the sense that the vertical length scale is much less than the horizontal one. We argue that the predominant vertical momentum balance in the current is hydrostatic and that viscous effects in the horizontal momentum balance are negligibly small. Hence the motion is governed by the balance between pressure and inertia forces in this horizontal direction. An order-of-magnitude analysis indicates that the perturbation of the upper free surface introduced by the flow can be neglected when $(\rho_c-\rho_a)/\rho_a \ll 1$, as assumed here. The pertinent shallow-water formulation is obtained in terms of two dependent variables, the z-averaged radial velocity $u(r,t)$ and the thickness of the current, $h(r,t)$. The details of the formulation are omitted here, but are similar to these presented in Ungarish & Huppert (1998, 2002).

The equations of motion can be conveniently expressed either in terms of h and the combined variable (uh) in conservation form, or in terms of the original variables in characteristic form, as follows.

3.1. *The governing equations*

In conservation form the equations can be written as

$$\frac{\partial h}{\partial t}+\frac{\partial}{\partial r}(uh)=-\frac{uh}{r}, \tag{6}$$

and

$$\frac{\partial}{\partial t}(uh) + \frac{\partial}{\partial r}\left[u^2 h + \tfrac{1}{2}h^2\right] = -\frac{u^2 h}{r}, \tag{7}$$

which in characteristic form become

$$\begin{bmatrix} h_t \\ u_t \end{bmatrix} + \begin{bmatrix} u & h \\ 1 & u \end{bmatrix} \begin{bmatrix} h_r \\ u_r \end{bmatrix} = \begin{bmatrix} -uh/r \\ 0 \end{bmatrix}. \tag{8}$$

Note the curvature term on the right-hand side of (8), which acts like a source or sink term, depending upon the sign. The contribution to the local time variation of h is negative (like a sink) for the conventional outward propagation situation, but becomes positive (like a source) for the inwardly propagating current discussed here. However, this term is not present for a rectangular x, z current (obtained by taking the limit $r \to \infty$ and then replacing r with x), and hence in this limit the only difference between an inwardly and outwardly propagating current is the direction of propagation.

3.2. *Characteristics and boundary conditions*

The characteristic paths and relationships provide useful information for the solution of the system, including a proper definition of boundary conditions for the interface height h at the ends of the current domain. Consider the equations of motion (8). Following the standard procedure for deriving characteristic relationships, we calculate the eigenvalues of the matrix of coefficients of the space-derivatives of the variables, which give the speeds of propagation as

$$\frac{\mathrm{d}r}{\mathrm{d}t} = \lambda_{\pm} = u \pm h^{1/2}, \tag{9}$$

and the corresponding eigenvectors

$$\left(\pm 1, h^{1/2}\right). \tag{10}$$

Consequently, the relationships between the variables on the characteristics with $\mathrm{d}x/\mathrm{d}t = \lambda_{\pm}$ are

$$\mathrm{d}h \pm h^{1/2}\,\mathrm{d}u = -\mathrm{d}t\,\frac{uh}{r}. \tag{11}$$

The initial conditions are zero velocity and unit dimensionless height and length at $t = 0$. Also, the velocity at $r = R$ is zero, and an additional condition is needed at the nose $r = r_N(t)$.

3.3. *The nose velocity*

The boundary condition for the velocity at the nose is essential for a proper physical definition and mathematical closure of the problem. The appropriate condition for the homogeneous ambient has been well studied, both theoretically and experimentally (Benjamin 1968; Huppert & Simpson 1980; Rottman & Simpson 1983). There is strong evidence that the velocity of the nose is proportional to the square-root of the pressure head per unit mass, and that the factor of proportionality, defined as the Froude number Fr, varies in a quite narrow range with the ratio h_N/H. We argue that this result reflects a local, quasi-steady integral property of the current head and hence it is expected to remain valid also for a circular geometry when the radius of curvature is large compared to the local height of the front. We therefore impose the

boundary condition

$$u_N = \frac{\mathrm{d}r_N}{\mathrm{d}t} = -Fr\ h_N^{1/2}. \tag{12}$$

Consistent with these considerations, we assume that the behaviour of Fr in the present case is approximated well by the well-known two-dimensional rectangular situation, as follows. Benjamin (1968) proved that Fr is a decreasing function of h_N/H. Experiments confirmed this qualitative behaviour, but also indicated that the theoretical value of Fr, derived by Benjamin (1968) for a highly idealized motion, needs some modifications (a reduction of typically 20%) in real circumstances. To reconcile theory with practice, Huppert & Simpson (1980) developed the following simple well-known correlation which we shall also use here:

$$Fr = \begin{cases} 1.19 & (0 \leqslant h_N/H \leqslant 0.075) \\ 0.5H^{1/3}h_N^{-1/3} & (0.075 \leqslant h_N/H \leqslant 1). \end{cases} \tag{13}$$

The scatter of the data used to obtain this formula suggests an estimate of $\pm 5\%$ for the error of this correlation, though later experiments and calculations by Rottman & Simpson (1983) suggest that, in some circumstances, the values for small h_N/H may be about 15% smaller than predicted by 13. These discrepancies appear because in real gravity currents various departures from the idealized model are unavoidable, such as the complex three-dimensional structure of the head, time dependence, turbulent mixing, entrainment, friction, etc. Although each one of these effects is expected to be small, their accumulated contribution may be significant. It is therefore unlikely that a more accurate general one-parameter simple fit can be obtained. We therefore adopt (13) as a prototype correlation in the following work, but it will be evident that the essence of the analysis and conclusions are not affected by small details of the functional form of $Fr(h_N/H)$.

This closes the SW formulation. In general, the resulting system requires a numerical solution for the partial differential equations, as follows.

3.4. *Numerical solution*

The hyperbolic governing equations (6)–(7) are formulated in conservation form for the variables h, $q = uh$, and are amenable to a numerical finite-difference solution by the classical two-step Lax–Wendroff method. A similar approach was used by, for example by Bonnecaze *et al.* (1993) and Ungarish & Huppert (1998), but here some modifications are necessary because of the unusual inward propagation. To facilitate the implementation of the boundary conditions, the r-coordinate is mapped to

$$y = \frac{r - r_N(t)}{R - r_N(t)}, \tag{14}$$

which keeps the physically expanding current in the fixed computational domain $0 \leqslant y \leqslant 1$. Consequently, the original equations (6)–(7) are subjected to the transformations

$$\left.\begin{aligned} \left(\frac{\partial}{\partial t}\right)_r &= \left(\frac{\partial}{\partial t}\right)_y - (1-y)\frac{\dot{r}_N}{R - r_N(t)}\left(\frac{\partial}{\partial y}\right)_t, \\ \left(\frac{\partial}{\partial r}\right)_t &= \frac{1}{R - r_N(t)}\left(\frac{\partial}{\partial y}\right)_t, \end{aligned}\right\} \tag{15}$$

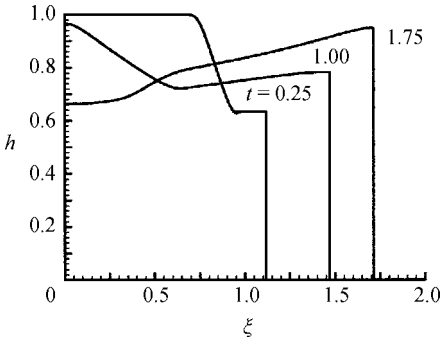

FIGURE 5. SW results for $H = 1$. The profile of h as a function of $\xi = R - r$ at various times for an inward current with $R = 2$.

where $\dot{r}_N = \mathrm{d}r_N/\mathrm{d}t$, see (12). The velocity of the characteristics (9) is also transformed through

$$\frac{\mathrm{d}y}{\mathrm{d}t} = \frac{1}{R - r_N(t)} \left[u \pm h^{1/2} - (1 - y)\dot{r}_N\right]. \tag{16}$$

The y-coordinate is discretized in constant-length intervals. The boundary conditions are applied at $y = 1$ (the outer wall of the container) and at $y = 0$ (the inward moving nose). The boundary conditions on the velocity, for each time step, are known explicitly, and the boundary conditions on h are calculated using the characteristic relationships (11) and (16). Each new time step $r_N(t)$ is updated using (12). Typically, we used 200 y-intervals and a time step of 0.002, but the convergence and resolution (accurate to at least three significant digits) has also been tested on finer grids.

4. Theoretical results

4.1. *Moderate R*

Some useful insights into the phenomenon under investigation are provided by first considering moderate values of R. The SW results for a typical inwardly propagating gravity current are shown in figure 5. The total height is $H = 1$, i.e. initially the height of the current is equal to that of the ambient. The outer radius is at $R = 2$, which implies that initially the nose of the current is only one lock length away from the axis, and hence the curvature effects, represented by the right-hand-side term in (6), are expected to be significant, even dominant, during the motion of the nose. Indeed, we observe in the figure that early in the motion ($t = 0.25$) the interface adjusts to the expected classical profile, with $h_N \approx 0.55$. However, at larger times the nose becomes higher. To contrast this behaviour of the inwardly propagating current, we present in figure 6 the behaviour of an axisymmetric outwardly propagating current and of a rectangular current with the same initial conditions. The height of the nose of the axisymmetric outwardly propagating current clearly decreases with time and distance of propagation, while the rectangular current is in the initial slumping phase, with constant h_N and u_N.

Insight into the qualitative interpretation of this unusual behaviour is obtained by following the characteristic from the interior (where $h = 1$ and $u = 0$) to the nose and recalling the balance along it given by (11). Note that for the inwardly propagating current we follow a negative characteristic which propagates to smaller r. At the

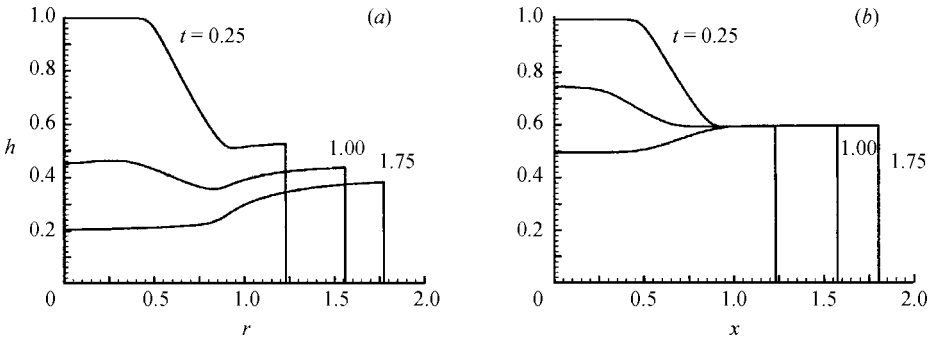

FIGURE 6. SW results for $H = 1$, at various times. (*a*) The profile of h as a function of r for an outwardly propagating axisymmetric current, and (*b*) h as a function of x for a rectangular current.

initial stage of the motion, while the time of propagation is small, the contribution of the source-like term on the right-hand side of (11) is negligible. This indicates that the curvature effects and the direction of propagation do not influence the relationship between dh and du at early times. In other words, the initial adjustments of nose height and (absolute) velocity are independent of curvature and direction of propagation. Eventually, the characteristic which reaches the nose travels for a longer time interval, and the curvature term affects the balance expressed in (11). First, differences between rectangular and circular or axisymmetric currents concerning the height of the nose during propagation begin to appear. Second, we notice that the source term is negative for outward radial motion, and positive for inward motion. Thus, this term contributes a decrease of h_N in the former case, and an increase in the latter case, which is emphasized here. Furthermore, for the inwardly propagating current r_N decreases with time and hence the influence of the curvature term is enhanced during the propagation.

Additional results are displayed in figure 7, for configurations with $R = 2$ and three representative values of H. In all cases the distance of propagation of the nose, ξ_N, increases (slightly) faster than linearly with time, t. This is, again, a result of the curvature term, whose influence increases when the radius, $r_N = R - \xi_N$, decreases. Indeed, both h_N and $|u_N|$ increase during the inward propagation. This trend is most pronounced for a deep current ($H = 15$), as a result of the Froude number dependence on h_N/H expressed by (13). For a deep current Fr is constant and hence $|u_N| \sim h_N^{1/2}$, but for a shallow layer of ambient fluid Fr varies and $|u_N| \sim h_N^{1/6}$. In any case, this behaviour is unusual, in the sense that the common classical gravity current is typified by a diminishing velocity of propagation and nose height.

The abovementioned features are less pronounced, but still relevant, when R, the container radius scaled with the gap of the lock, is large. The right-hand-side term in (6) is positive for inward motion, and effectively a source for increasing h during propagation, but this contribution competes with the spreading of the current by advection. The question is: which effect dominates? Since initially $r_N = R - 1$, the initial contribution of the curvature term in (6) is proportional to $(R-1)^{-1}$. Thus, for a large R the spread by advection is initially dominant, and the initial propagation is expected to be as in the rectangular case. However, since $r_N = R - \xi_N$ decreases during propagation, eventually the current nose reaches a region where the curvature source term plays a significant role (under the assumption that viscous effects remain small.)

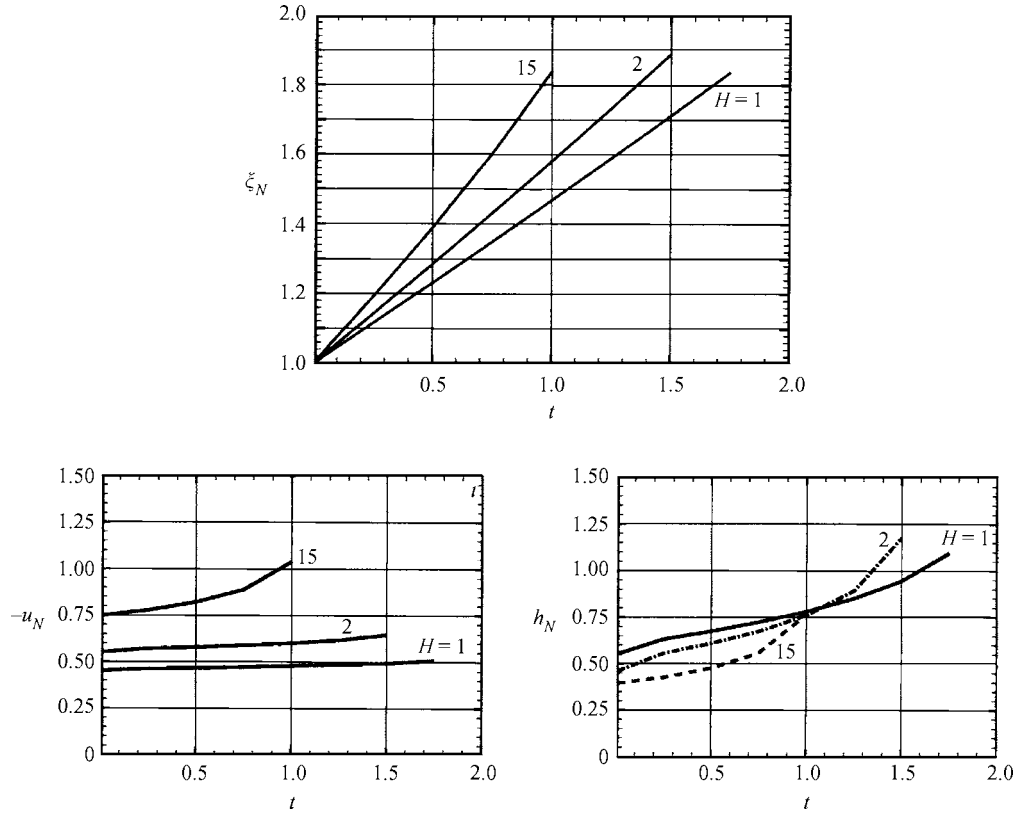

FIGURE 7. SW results for $R=2$: ξ_N, $-u_N$ and h_N as functions of t for various H.

An order-of-magnitude analysis of (6) is helpful. Using $r=R-\xi$ and the estimate $\partial(uh)/\partial\xi \approx (uh)/\xi$ we obtain

$$\frac{\partial h}{\partial t} \approx uh\left(\frac{1}{\xi}-\frac{1}{R-\xi}\right). \tag{17}$$

This indicates that the curvature term starts to affect the behaviour of the interface when the current head approaches the centre, $R/2$, and that the right-hand side changes sign there. This means that during the propagation in the region $\xi > R/2$ the usual trend of decaying h_N by spreading of the gravity current is reversed by the contribution of the converging geometry. We have confirmed these conclusions, derived from the simple estimate (17), by numerous numerical integrations of the SW equations.

These features are clearly observed in the behaviour of an inversely propagating current with $R=10$ and $H=1$, as displayed in figure 8. The initial curvature effects at the nose are $\sim (R-1)^{-1}$, i.e. in this case about nine times smaller than for the $R=2$ case. The nose first descends, but after it passes (approximately) the centre of the gap its height increases, as expected. The steady state of h at $\xi \approx 5$, as predicted by (17), is evident. A similar trend, but less pronounced, is observed for the velocity of propagation.

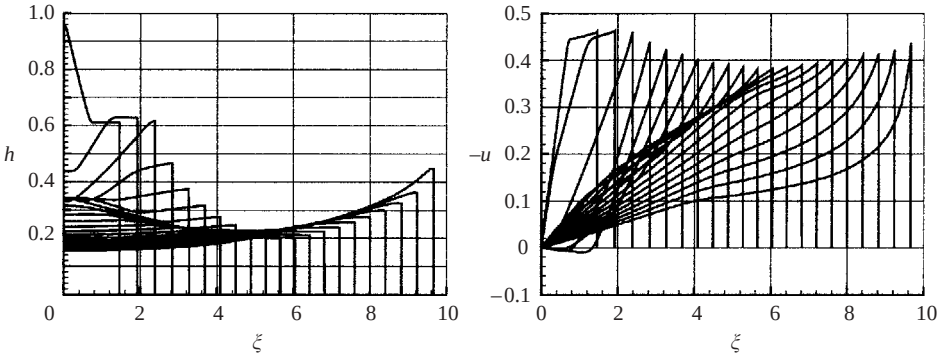

FIGURE 8. SW results for an inverse current configuration with $R = 10$ and $H = 1$. The profiles of h and u as a function of $\xi = R - r$ at various times $t = 1$ (1) 21.

We remark that the configurations with $H = 1$ are used here as a representative example of the general behaviour of the gravity current. Actually, when H is close to 1 the return flow in the upper layer may be influential during the initial and final stages of the motion, and hence a more accurate description may require a two-layer model formulation. The $h_N > H = 1$ result for $t > 1.7$ in figure 7 seems non-physical. A more detailed discussion is postponed to § 5.

4.2. *Comparisons with experiment*

The experiments provide direct measurements of the position of the nose as a function of time. Comparisons of the SW and experimental results of ξ_N as a function of time are shown in figures 9(*a–d*). Each plot is for a different value of R, and $H = 1$ for all cases, with the addition of one case with $H = 2.8$ in the plot for $R = 17.7$, figure 9(*b*). The value of the instantaneous nose Reynolds number (during the entire propagation) in the experiments presented was larger than 150 and hence we estimate that viscous effects were of little significance during most of the period of propagation. In figure 9(*a*) we present experiments 17, 18 and 21, with increasing values of Re_0, and observe good convergence with respect to this parameter.

The velocity of propagation as a function of time or position, which we attempted to evaluate from the measurements of $\xi_N(t)$, has considerable scatter and large possible errors. Typical results are shown in figure 10. Detailed comparison of this derived experimental variable with the theoretical prediction is inconclusive. However, there is fair agreement concerning magnitude and general trends. For the $R = 9.6$ cases, which are less exposed to viscous influence, see (A 10), we can discern in some of the experiments a tendency of increasing u_N in the second half of the gap. On the other hand, (A 10) indicates that in the experiments with $R = 37$ the viscous bottom friction dominates when $\xi_N > 20$, and, indeed, there is a remarkable discrepancy in the trend of u_N between experiment and theory for $\xi > 26$.

Overall, the comparison of our experiments with the SW results is very encouraging. The qualitative agreement is very good. The experimental data collapse well according to the scaling and the key dimensionless parameters R and H indicated by the theory. The theoretical prediction that the nose velocity variations are small so that an almost constant u_N prevails in many cases has clear experimental support. The predicted increase of u_N as the current nose approaches the centre is, however, not clearly observed in the experimental data, but this effect is numerically quite small in the cases presented, and, again, the accuracy of the experimental velocity, obtained by

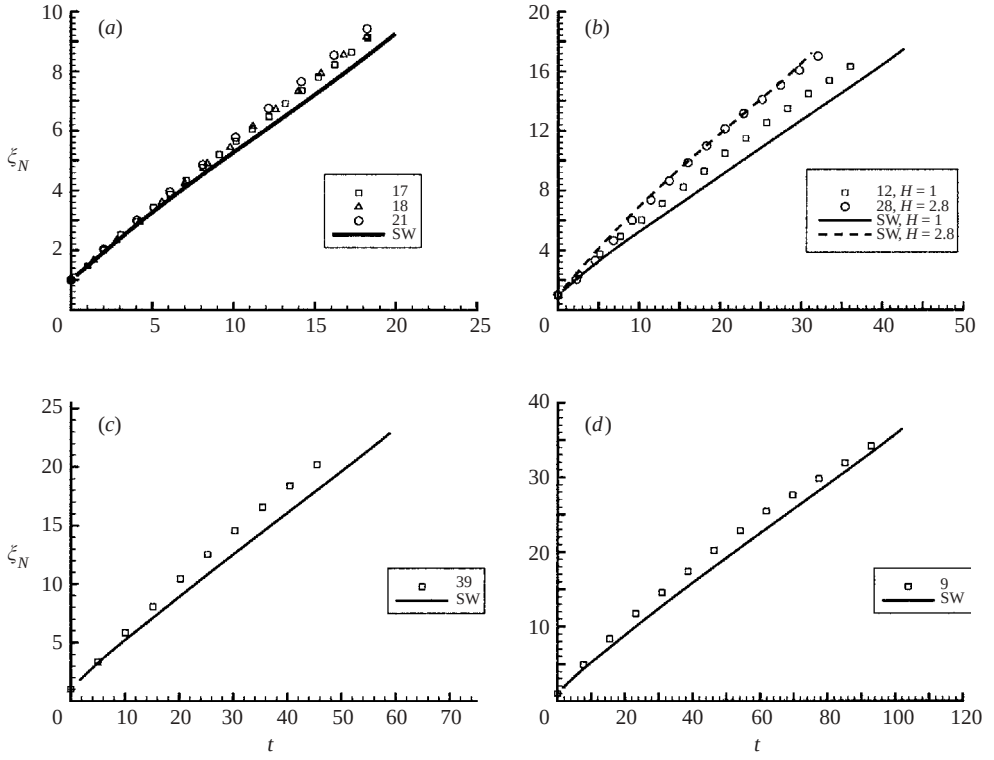

FIGURE 9. Experimental (symbols) and SW (lines) results for ξ_N as functions of t. The legends indicate the number of the experiment, and also the value of H when different from 1. (*a*) $R = 9.5$, (*b*) $R = 17.7$, (*c*) $R = 23.4$, (*d*) $R = 36.9$.

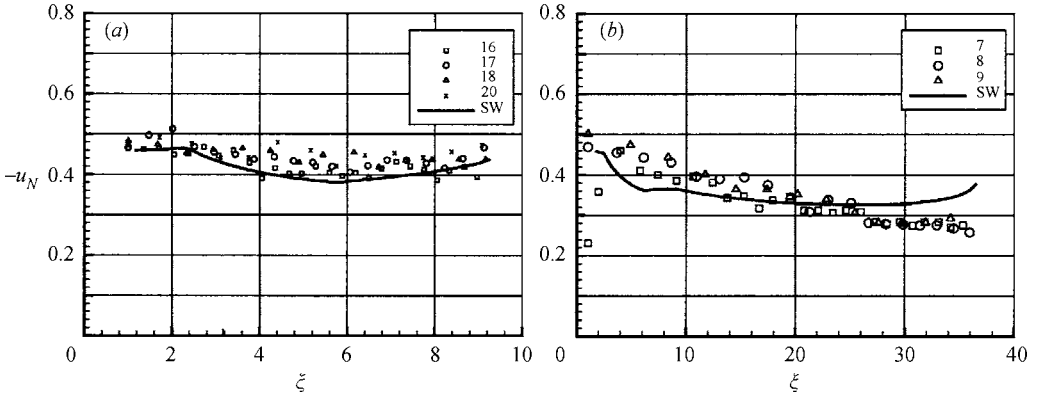

FIGURE 10. Experiment and SW results for $-u_N$ as a function of ξ, for (*a*) $R = 9.6$ and (*b*) 37. In all cases $H = 1$.

numerical differentiation of distance data, is low. The SW and experimental results are in agreement on the influence of the total depth, i.e. the speed of propagation increases as H increases. (Unfortunately, however, this relationship could not be qualitatively verified for values of H larger than 2.8 because the corresponding experiments were affected by viscous terms.)

Quantitatively, there are discrepancies of typically 10% in the behaviour of the distance of propagation as a function of time. The SW predictions for $H = 1$ have the tendency to underpredict the propagation. However, the discrepancy is not systematic, see figure 9: for experiment 17 (with $H = 1$) the SW results underpredict $\xi(t)$ for all t, but for experiment 28 (with $H = 2.8$) the opposite is detected for $t < 15$ and $t > 25$.

The discrepancies between the experimental and SW results can be attributed to various factors. First, there are intrinsic incompatibilities between the theoretical idealization and the practical apparatus: the experimental container was a wedge and obviously the sidewalls introduced some deviations from the axisymmetric assumption; there were some vortical motions generated at the sidewalls; the lock gate is removed in a finite time, etc. Second, the SW theory is only an approximation, and reliant on the Froude condition (13) which is a curve-fit correlation involving some scatter in the data. Moreover, we employed the one-layer simplification whose deficiencies, in particular for $H = 1$, are discussed later. Finally, the experimental cases with larger R were affected by viscous friction in the second half of the gap. We therefore infer that the observed discrepancies are within the expected margin of accuracy of this type of investigation.

We believe that the overall agreement between the experimental data and the theoretical results is good, perhaps the best that can be hoped for with the employed experimental and theoretical techniques.

4.3. *Large R 'numerical experiment'*

The laboratory experiments discussed in § 2 covered a range in R of 9.6–37, and the agreement with the SW numerical results gives credence to this predictive tool. The extension of the insights to the range of large R is of interest, but laboratory experiments for this parameter range would be difficult. We attempt to cover this gap by numerical experimentation, as follows. Here we use input data for configurations corresponding to the experimental data of table 1, but for a container with outer radius three times larger than used in the laboratory (i.e. 702 cm in dimensional form). This results in a value of R three times larger than in the corresponding laboratory experiment, but the other initial conditions remain unchanged.

The propagation features of a current with $R = 53.2$ (three times larger than in experiments 10, 27, 29, 30) are displayed in figure 11. The overall propagation ξ_N as a function of t, is, after some initial adjustment, almost a straight line. The initial propagation is slightly faster for larger values of H. The plots of u_N and h_N as a function of t provide more details. After an initial decay of h_N ($0 < t < 30$) the current enters a mode of propagation with almost constant h_N and u_N. The value of u_N during this stage is about half of the initial value. This is indeed remarkable, because by conservation of volume the average thickness decays by a factor of about 26 as ξ_N increases from 1 to 51. Moreover, as the nose approaches the centre both h_N and u_N increase.

Figure 12 shows the behaviour of h_N and u_N as functions of the distance of propagation $\xi_N(t)$ for configurations with $H = 1$ and various R (in the range 28.9–111). The abovementioned typical features are clearly observed for all values of R considered. However, as R increases the curvature terms effects become monotonically less pronounced during the main interval of propagation. This is expected, because the curvature terms become important at $\xi_N \approx R/2$, and until this stage is reached the current head monotonically decelerates. For example, the minimum $|u_N|$ is 0.34 for $R = 28.9$, but 0.20 for $R = 111$.

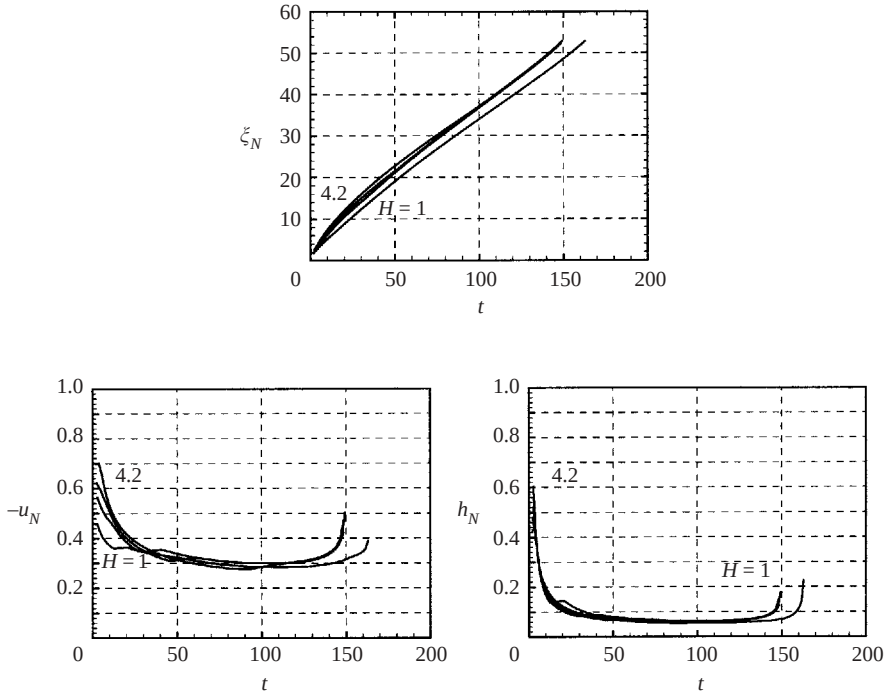

FIGURE 11. SW results for $R = 53.2$: ξ_N, $-u_N$ and h_N as functions of t for $H = 1, 2, 2.8$ and 4.2.

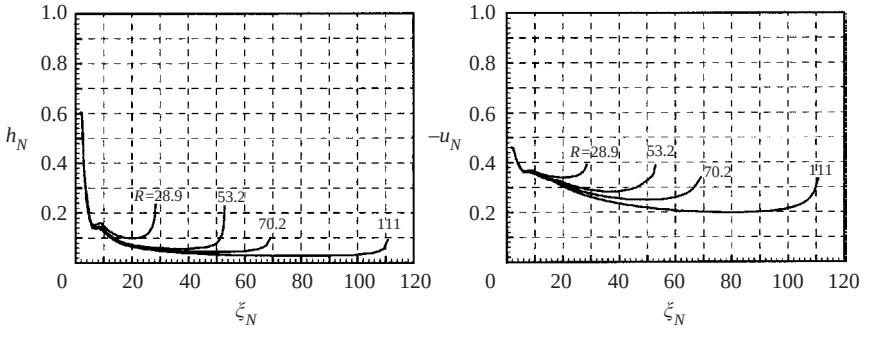

FIGURE 12. SW results for $H = 1$: $-u_N$ and h_N as functions of ξ_N for various R.

The decay of both the nose velocity and height is accompanied by a decrease of the effective nose Reynolds number, which, although less dramatic than in the outward propagation process, may lead to violation of the inviscid assumption in practical circumstances. For example, in experiment 14 the reference height h_0 and velocity U, see (3), are 9.45 cm and 10.0 cm s^{-1}, respectively, and $\nu = 10^{-2}$ cm^2 s^{-1}. In the corresponding numerical experiment with $R = 111$, see figure 12, the value of $u_N^* h_N^*/\nu$ (the asterisks denote dimensional variables) reaches the minimum of 53 when $\xi_N = 90$. This is near the margin of the inviscid domain for gravity currents.

5. Concluding remarks

The combined experimental and theoretical study of an inwardly propagating gravity current provides some novel insights. It is well known that an outwardly propagating axisymmetric gravity current, attains, after some adjustment time, a self-similar behaviour during which the speed of propagation and the height of the nose decay monotonically with time. On the other hand, we showed that an inwardly propagating gravity current displays initially a weaker decay of both $|u_N|$ and h_N, and, eventually, a slight increase of both these variables. Overall, the propagation maintains a fairly constant speed for a considerable time interval. We proved that these differences are curvature effects on the flow in the vicinity of the nose, represented by the term $-uh/r$ on the right-hand side of the governing equation for $h(r, t)$. For an outwardly propagating current this term is negative and decays with time, but for the inwardly propagating current this term is positive and its contribution increases with time.

An extension of the SW one-layer theoretical model to this problem was developed. The SW predictions of the distance of propagations as function of time are in good agreement with the experiments. However, the predicted increase of $|u_N|$ and h_N near the apex were not supported by the experimental observations. A box-model approximation was also considered (Appendix). This approach is able to provide an approximation of the motion, but misses the different trends for inward and outward motions when the nose is in the second half of the gap of propagation. The box-model predictions of the distance of inviscid propagation (start of viscous term dominance) is consistent with the experimental data.

It is remarkable that the semi-empirical Froude conditions (13) developed for quite simple two-dimensional rectangular cases serve well, without noticeable loss of accuracy, in the present case where curvature effects play an important role. This strengthens the argument that propagation of the nose is determined by local balances.

Our theoretical analysis used a one-layer SW model, which must be considered a first step in the investigation. Recent studies indicate that the return flow in the upper layer may influence the motion of the dense current, in particular for $H < 2$; to reproduce these details a complex two-layer SW model must be employed, see Bonnecaze *et al.* (1993), Klemp *et al.* (1994) and Ungarish & Zemach (2003). An important detail that is missed by the one-layer model is the fact that the velocity λ of the characteristic towards the nose decreases with H so fast that for $H < 1.2$ (approximately) the attainable nose velocity is constrained (choked) by the value of λ (to prevent cavitation). In our case the constraint yields $|u_N| \approx 0.43H$. An inspection of the one-layer results in the cases under consideration shows that this limitation has not been violated. Moreover, in axisymmetric configurations that constraint is relevant only for a short initial time interval. Thus, we expect the one-layer results to remain a fair approximation even for the experiments with $H = 1$. The two-layer SW investigation remains a challenge which is left for future investigation, and is expected to improve the agreement with experiments.

When the nose reaches the vicinity of the centre, the shallow-water approximation becomes invalid as the current hits the axis and reacts with it. The behaviour at this stage and at subsequent times is an interesting topic, left for future study.

The research was supported by NERC and by the Fund for Promotion of Research at the Technion.

Appendix. Box-model simplification

Box models are simple momentum-integral-type approximations of the behaviour of gravity currents. There is evidence that they provide reasonably accurate results for the distance and velocity of propagation as a function of time in the classical cases of two-dimensional and outwardly axisymmetric spreading. Here we attempt to assess the predictive value of this tool for the inwardly propagating current.

Following the classical procedure, we consider the gravity current as an annular volume of height $h_N(t)$ independent of r. The prescribed conditions are volume conservation,

$$\tfrac{1}{2}h_N(t)\left[R^2 - r_N^2(t)\right] = V = \text{const}, \tag{A 1}$$

and the nose velocity correlation,

$$\frac{\mathrm{d}r_N}{\mathrm{d}t} = -Fr(h_N)h_N^{1/2}(t), \tag{A 2}$$

where, again, R is the outer radius of the container, Fr is given by (13) and the volume V (in dimensionless form per radian) is given by

$$V = \tfrac{1}{2}[R^2 - (R-1)^2] = R - \tfrac{1}{2}. \tag{A 3}$$

From (A 1) and (A 3) we obtain $h_N(t)$ as a function of $r_N(t)$, then substitute in (A 2) to obtain one ordinary differential equation for $r_N(t)$. However, we must distinguish between the different behaviours of $Fr(h_N)$, see (13), and we obtain

$$\frac{\mathrm{d}r_N}{\mathrm{d}t} = -0.5H^{1/3}\left[\frac{2R-1}{R^2 - r_N^2}\right]^{1/6} \qquad \left(\frac{h_N}{H} \geqslant 0.075\right), \tag{A 4}$$

$$\frac{\mathrm{d}r_N}{\mathrm{d}t} = -1.19\left[\frac{2R-1}{R^2 - r_N^2}\right]^{1/2} \qquad \left(\frac{h_N}{H} \leqslant 0.075\right), \tag{A 5}$$

subject to the initial condition

$$r_N = R - 1 \qquad (t = 0) \tag{A 6}$$

(in fact, the expression in the square brackets is h_N). These equations can be integrated to obtain $r_N(t)$. The analytical result is awkward, but the numerical quadrature is straightforward.

Some useful observations can already be made. Since $r_N(t)$ decreases, the (absolute) velocity of propagation, $|\mathrm{d}r_N/\mathrm{d}t|$, predicted by (A 4)–(A 5) decreases monotonically with t. This indicates that the box model must become inconsistent with the SW predictions when the nose is in the second half of the interval, $r_N < R/2$.

Some detailed comparisons of the box model with SW results for various configurations are presented in figures 13 and 14. The results are partly disappointing. There is good agreement in $\xi(t)$ for moderate values of R and non-large H. The trend of $|u_N|$ to decrease with time, at the beginning of the propagation, is also correctly reproduced by the box model. However, the box model is unable to predict the trend of $|u_N|$ to increase in the later stage of propagation. The SW and experimental results show that, eventually, the deceleration of $|u_N|$ stops and is even reversed, for both a deep and shallow current.

This discrepancy is caused by an basic property of the box-model formulation: because it assumes spreading with uniform height, h_N must be a monotonically decreasing function of t for both outwardly and inwardly propagation. This trend of decrease carries over to u_N, which is proportional to h_N (to some positive power).

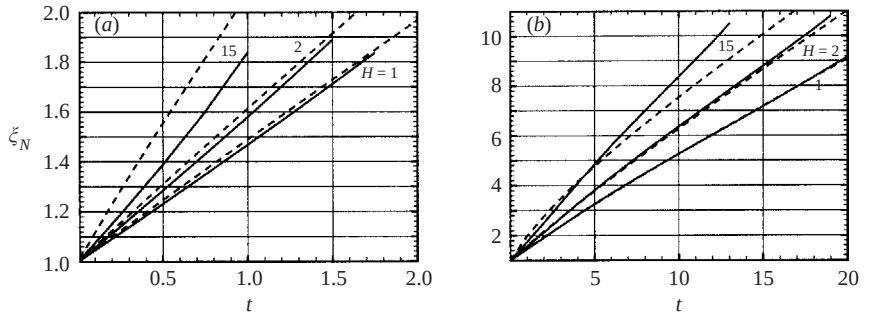

FIGURE 13. Propagation distance as functions of t: box model (dashed line) and SW (solid line) results for (*a*) $R = 2$ and (*b*) $R = 11$, various H.

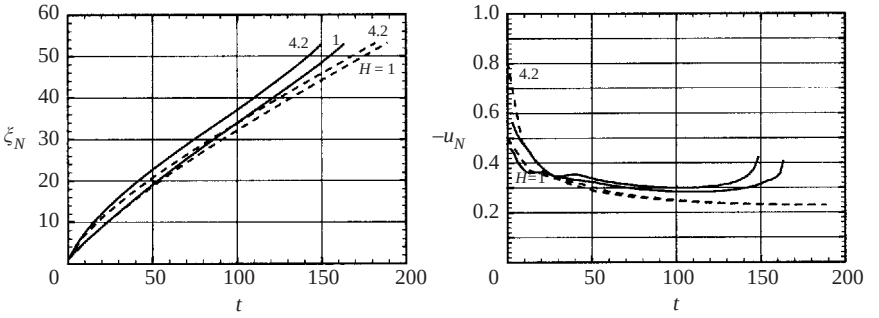

FIGURE 14. Propagation distance and nose velocity as functions of t: box model (dashed line) and SW (solid line) $R = 53.2$, $H = 1$ and 4.2.

Thus, to obtain the correct behaviour of the gravity current it is necessary to consider the coupling between continuity and momentum conservation.

Estimates of the relative importance of global forcing terms can be also obtained. The (dimensional) inertial force per radian is

$$F_i \sim \rho U^2 \xi_0 h_0 V \frac{u_N^2}{\xi_N} \tag{A 7}$$

and, similarly, the viscous bottom friction is

$$F_v \sim \rho \nu U \frac{\xi_0^2}{h_0} \frac{u_N}{h_N} \frac{V}{h_N}, \tag{A 8}$$

where $\sim$ denotes order of magnitude. The ratio of these forces is

$$\frac{F_v}{F_i} \sim \frac{1}{Re_0} \frac{\xi_0}{h_0} \xi_N \frac{1}{u_N h_N^2} \sim \frac{1}{Re_0} \frac{\xi_0}{h_0} \xi_N^{7/2}, \tag{A 9}$$

upon use of $u_N^2 \sim h_N$, $h_N \sim \xi_N^{-1}$ and $Re_0 = U h_0 / \nu$.

The viscous effect is therefore expected to become dominant when that ratio is larger than 1, i.e.

$$\xi_N > \xi_V = [Re_0 (h_0/\xi_0)]^{2/7}. \tag{A 10}$$

The typical ξ_V in our experiments is 15 and therefore some significant viscous influence is expected in the experimental cases with larger R, in particular for $R = 36.9$. The values of ξ_V/R are shown in table 1; it turns out that there is a correspondence between the theoretical $\xi_V/R < 0.5$ and the label V derived from subjecting the experimental data to the condition that the local Reynolds number becomes smaller than 100 during the propagation.

REFERENCES

Abgenent, S. B. & Aronson, D. G. 1995 Intermediate asymptotics for convergent viscous gravity currents. *Phys. Fluids* **7**, 223–225.

Barenblatt, G. I. 1996 *Scaling, Self-similarity, and Intermediate Asymptotics.* Cambridge University Press.

Benjamin, T. 1968 Gravity currents and related phenomena. *J. Fluid Mech.* **31**, 209–248.

Bonnecaze, R. T., Hallworth, H. A., Huppert, H. E. & Lister, J. R. 1995 Axisymmetric particle-driven gravity currents. *J. Fluid Mech.* **294**, 93–121.

Bonnecaze, R. T., Huppert, H. E. & Lister, J. R. 1993 Particle-driven gravity currents. *J. Fluid Mech.* **250**, 339–369.

Diez, J. A., Gratton, R. & Gratton, J. 1992 Self-similar solutions of the second kind for a convergent viscous gravity current. *Phys. Fluids* A **4**, 1148–1155.

Hogg, A. J., Hallworth, M. A. & Huppert, H. E. 1999 Reversing buoyancy of particle-driven gravity currents. *Phys. Fluids* **11**, 2891–2900.

Huppert, H. E. 1982 The propagation of two-dimensional and axisymmetric viscous gravity currents over a rigid horizontal surface. *J. Fluid Mech.* **121**, 43–58.

Huppert, H. E. 1998 Quantitative modelling of granular suspension flow. *Phil. Trans. R. Soc. Lond.* A **356**, 2471–2496.

Huppert, H. E. 2000 Geological fluid mechanics. In *Perspectives in Fluid Dynamics: A Collective Introduction to Current Research* (ed. G. K. Batchelor, H. K. Moffatt & M. G. Worster), pp. 447–506. Cambridge University Press.

Huppert, H. E. & Simpson, J. E. 1980 The slumping of gravity currents. *J. Fluid Mech.* **99**, 785–799.

Klemp, J. B., Rotunno, R. & Skamarock, W. C. 1994 On the dynamics of gravity currents in a channel. *J. Fluid Mech.* **269**, 169–198.

Rottman, J. & Simpson, J. 1983 Gravity currents produced by instantaneous release of a heavy fluid in a rectangular channel. *J. Fluid Mech.* **135**, 95–110.

Simpson, J. E. 1997 *Gravity Currents in the Environment and the Laboratory*. Cambridge University Press.

Ungarish, M. & Huppert, H. E. 1998 The effects of rotation on axisymmetric particle-driven gravity currents. *J. Fluid Mech.* **362**, 17–51.

Ungarish, M. & Huppert, H. E. 2002 On gravity currents propagating at the base of a stratified ambient. *J. Fluid Mech.* **458**, 283–307.

Ungarish, M. & Zemach, T. 2003 On the slumping of high Reynolds number gravity currents in two-dimensional and axisymmetric configurations. *Eur. J. Mech.* B *Fluids* (submitted).